A NEW SOLUTION FOR THE DEFORMATIONS OF AN INITIALLY ELLIPTICAL ELASTIC-WALLED TUBE

by D.J Netherwood *and* R.J Whittaker

(*School of Mathematics, The University of East Anglia, Norwich Research Park, Norwich, United Kingdom, NR4 7TJ.*)

[Received May 2022 , Accepted Oct 2022]

Abstract

We investigate the small-amplitude deformations of a long thin-walled elastic tube having an initially axially uniform elliptical cross-section. The tube is deformed by a (possibly non-uniform) transmural pressure. At leading-order its deformations are shown to be governed by a single partial differential equation (PDE) for the azimuthal displacement as a function of the axial and azimuthal co-ordinates and time. Previous authors have obtained solutions of this PDE by making ad-hoc approximations based on truncating an approximate Fourier representation. In this paper, we instead write the azimuthal displacement as a sum over the azimuthal eigenfunctions of a generalised eigenvalue problem, and show that we are able to derive an uncoupled system of linear PDEs with constant coefficients for the amplitude of the azimuthal modes as a function of the axial co-ordinate and time. This results in a formal solution of the whole system being found as a sum over the azimuthal modes. We show that the nth mode's contribution to the tube's relative area change is governed by a simplified second-order PDE, and examine the case in which the tube's deformations are driven by a uniform transmural pressure. The relative errors induced by truncating the series solution after the first and second term are then evaluated as a function of both the ellipticity and pre-stress of the tube. After comparing our results with Whittaker et al (Q. J. Mech. Appl. Math. **63**(4) 465-496, 2010), we find that this new method leads to a significant simplification when calculating contributions from the higher-order azimuthal modes, which in turn makes a more accurate solution easier to obtain.

1. Introduction

The fluid–structure interaction between elastic-walled tubes and biological fluids can be observed throughout the biological sciences. In the circulatory system, pulse–wave propagation allows for the transportation of nutrients to tissues and organs within the body (**1**), and it is flow-induced deformations that lead to the rupture of arterial and cerebral aneurysms (**2**). In the respiratory system, there is a strong interaction between air flow and the elasticity of the airway walls, leading to physiologically significant flow limitation (**3**). To construct mathematical models that capture such physiological behaviour, we must consider both the mechanics of the internal fluid, and the mechanics of the tube wall.

Many theoretical models that describe the relationship between the deformation of elastic-walled tubes and the fluid conveyed within them are based on experimental models. These models are generally based on what has become a canonical set-up known as the 'Starling resistor' (**4**). The typical set-up is shown in Fig. 1 and consists of a thin-walled, finite-length (but not necessarily axially uniform) elastic tube. The tube is pre-stretched and pinned (at

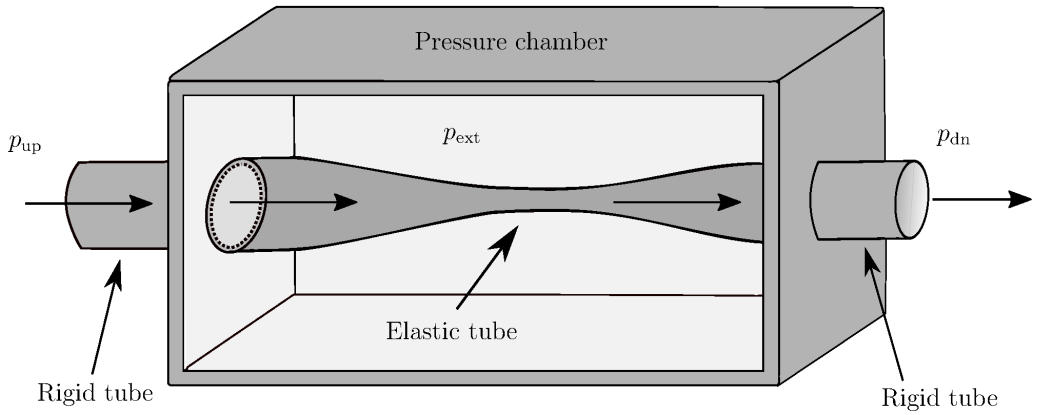

Figure 1: The typical set-up of the Starling resistor comprising a thin-walled elastic tube section pinned between two rigid tubes. The elastic section is placed inside a pressure chamber and fluid is driven through the system by either imposing a pressure difference between the ends of the tube or by imposing a flow rate at one end using a volumetric pump.

both ends) to two rigid tubes. Fluid is driven through the system by either imposing a pressure difference between either end of the tube, or by imposing a flow rate at one end through a volumetric pump. By placing the collapsible section of the tube inside a pressure chamber, we are given the freedom to manually alter the ambient pressure that imposes a force on the exterior of the tube. By ensuring that the external pressure p_{ext} is larger than the interior fluid pressure p_{int} by a suitable amount, the transmural pressure $p_{\text{int}} - p_{\text{ext}}$ will be sufficiently negative to induce buckling. For large positive transmural pressures (applicable for most arteries), the tube is inflated and the transmural pressure is mainly balanced by an azimuthal hoop stress. When the transmural pressure decreases, the tube's cross-section becomes elliptical-like, and the compliance of the tube increases. Decreasing the transmural pressure further causes the tube's cross-section to adopt a 'two lobed' state (see Fig. 2) before the opposite sides finally come into contact (**5**). In its deformed state, small changes in the transmural pressure yields large changes in cross-sectional area, and in this state, the system will often exhibit self-excited oscillations in the presence of an axial flow (**3**).

The simplest theoretical approach to understanding the interaction between compliant elastic-walled tubes and the fluid conveyed within them is via a one-dimensional model. The conservation of both mass and axial momentum of the internal fluid provide two equations relating the internal pressure p_{int}, the fluid velocity u, and the tube's cross-sectional area A. To close the system, we require a third and final equation — known as a 'tube law' — that captures the mechanics of the elastic-walled tube. The tube law, which usually takes the form

$$p_{\text{int}} - p_{\text{ext}} = P(A), \tag{1.1}$$

for some function P, is often chosen to fit experimental results.

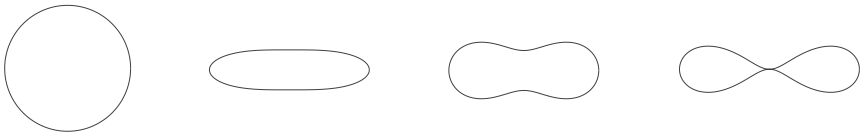

Figure 2: Typical cross-sectional shapes of an elastic-walled tube subject to increasingly negative (left to right) transmural pressures $p_{\text{int}} - p_{\text{ext}}$. The first (circular) cross-section corresponds to a positive transmural pressure, whilst the remaining cross-sections all correspond to negative transmural pressures.

Flaherty *et al.* (**6**) was one of the first to propose a tube law, based on the post-buckling behaviour of an inextensible elastic ring. However, this local analysis fails to capture axial tension effects that are induced by the interaction with neighbouring cross-sections (**7**). In an attempt to improve the tube law of Flaherty *et al.* (**6**), many authors have proposed ways of incorporating contributions from axial forces and bending moments. We refer the reader the studies (**8**), (**9**), (**5**), (**10**) and (**11**) as examples.

In the present work we will adopt the initial modelling of Whittaker *et al.* (**10**), who investigated the small-amplitude deformations of a long thin-walled elastic tube having an initially axially uniform elliptical cross-section. The deformations of the tube were assumed to be induced by an azimuthally uniform transmural pressure, and contributions from the inertia of the tube wall were ignored. Whittaker *et al.* (**10**) formally derived governing equations using Kirchhoff–Love shell theory within a long wavelength thin-walled regime, and then used these to obtain a tube law.

By considering the equilibrium of forces in the normal, azimuthal and axial directions, together with linear constitutive laws, Whittaker *et al.* (**10**) formulated the entire problem in terms of an azimuthal displacement $\eta(\tau, z)$, which depends on the azimuthal co-ordinate τ and axial co-ordinate z. The governing PDE for η was shown to be of the form

$$\mathscr{L}\left(\mathscr{K}(\eta)\right) - \tilde{F}\frac{\partial^2}{\partial z^2}\mathscr{J}(\eta) = \tilde{P}(z)C_P h, \tag{1.2}$$

where $\mathscr{L}, \mathscr{K}$ and $\mathscr{J}$ are linear differential operators in τ, $\tilde{F}$ is the dimensionless axial tension, and $\tilde{P}(z)$ is the dimensionless (azimuthally uniform) transmural pressure. The quantities $C_P(\tau)$ and $h(\tau)$ are known functions of the azimuthal coordinate τ and arise during the set-up of the problem.

Whittaker *et al.* (**10**) opted to solve (1.2) via Fourier decomposition, by seeking a solution of the form

$$\eta(\tau, z) = \sum_{n=1}^{\infty} e_n(z)\sin(2n\tau). \tag{1.3}$$

Whittaker *et al.* (**10**) argued that just the first term in (1.3) would provide a good approximation to η. After truncating (1.3) after mode $n = 1$ and introducing $\alpha(z)$, the relative change in cross-sectional area, Whittaker *et al.* (**10**) deduced the tube law

$$\tilde{P} = k_0\alpha - k_2\tilde{F}\frac{\mathrm{d}^2\alpha}{\mathrm{d}z^2}, \tag{1.4}$$

where k_0 and k_2 are constants, which are computed using numerical solutions for the leading Fourier modes of the particular integral and complementary function of (1.2).

Walters *et al.* (**12**) furthered the work of Whittaker *et al.* (**10**) by including contributions due to the inertia of the tube wall. Walters *et al.* (**12**) showed that such contributions could be captured via a single parameter M, a dimensionless measure of the inertia in the tube wall. It was found that wall inertia contributed additively to the governing PDE (1.2) through a new term proportional to M. The governing equation becomes

$$\mathscr{L}\left(\mathscr{K}(\eta)\right) - \tilde{F}\frac{\partial^2}{\partial z^2}\mathscr{J}(\eta) + M\frac{\partial^2}{\partial t^2}\hat{\mathscr{J}}(\eta) = \tilde{P}(z)C_P h, \tag{1.5}$$

and the corresponding tube law is

$$\tilde{P} = k_0\alpha - k_2\tilde{F}\frac{\partial^2\alpha}{\partial z^2} + k_2 M\frac{\partial^2\alpha}{\partial t^2}. \tag{1.6}$$

Whilst the approach of Whittaker *et al.* (**10**) and Walters *et al.* (**12**) appeared to give good results, an ad-hoc approximation was used to truncate the Fourier series (1.3). The correction to the first mode, which is induced by the (coupled) higher-order modes is then difficult the calculate. In the present work, we will instead use an eigenfunction expansion method that allows the equations for the modes to fully decouple. We derive a formal solution of the whole system, which allows us to calculate the order of magnitude of the error induced after truncation at any mode.

We organise this paper as follows. In §2 we adopt the set-up of Whittaker *et al.* (**10**) by defining the geometry of the tube as well as the functions which measure wall deformation. A revised governing equation for $\eta(\tau, z, t)$ that permits azimuthal variation in the pressure is then presented. In §3 we introduce a generalised eigenvalue problem, which will later be used to decouple the governing equation for the azimuthal deformation. The generalised eigenvalue problem is solved numerically using a collocation method (`bvp4c`) and solutions for a variety of elliptical cross-sections are presented. In §4 we show that the relative area change α can be decomposed as $\alpha(z,t) = \sum_{n=1}^{\infty}\alpha_n(z,t)$, where each $\alpha_n(z,t)$ satisfies a tube-law like equation

$$\tilde{F}\frac{\partial^2\alpha_n}{\partial z^2} - M\frac{\partial^2\alpha_n}{\partial t^2} - \lambda_n\alpha_n = -Q_n(z,t)t_n. \tag{1.7}$$

Here α_n is the component of the relative area change corresponding to the nth azimuthal deformation eigenmode, λ_n and t_n are positive constants that arise from the solutions of the generalised eigenvalue problem, and $Q_n(z,t)$ measures forcing from the transmural pressure on the nth eigenmode. In §5 we examine the case where the deformations of the tube wall are induced by a steady uniform transmural pressure. In this case, the components $\alpha_n(z)$ are governed by a system of ordinary differential equations. We present results for the first four modes of the relative area change, comparing directly with the work of Whittaker *et al.* (**10**), and evaluate the relative error after truncation after $n = 1$ and $n = 2$. Finally, in §6 we present our final discussions and conclusions, whilst also commenting on future work.

2. Set-up

2.1 *Physical set-up*

We adopt the set-up of Whittaker *et al.* (**10**) and Walters *et al.* (**12**) by considering a long thin-walled elastic tube of length L, with mass per unit area m and wall thickness d

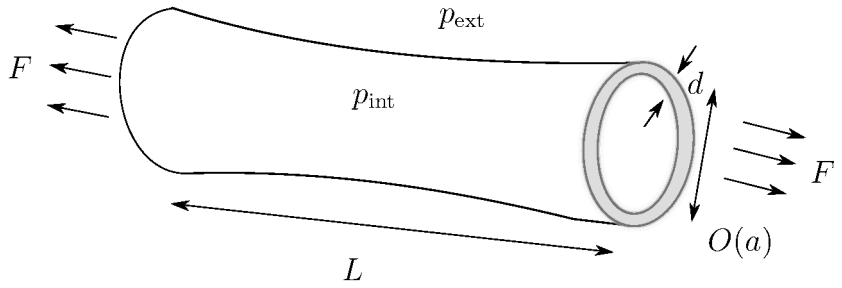

Figure 3: The typical set-up showing a long thin-walled tube of length L, mass per unit area m, and wall thickness d, with an initially axially uniform elliptical cross-section of circumference $2\pi a$. The tube is subject to an axial pre-stress $F/(2\pi ad)$ and is exhibiting deformations in response to an applied transmural pressure $p_{\text{int}} - p_{\text{ext}}$.

(see Fig. 3). In what we shall term the undeformed configuration, the tube is subject to an axial pre-stress of magnitude $F/(2\pi ad)$ and is axially uniform with an elliptical cross-section of circumference $2\pi a$. Hence F is the extensional force applied at the ends of the undeformed tube, and a is the length scale of the tube's cross-section. The tube is aligned with Cartesian coordinates (ax, ay, Lz) where z is aligned with the tube's central axis. We introduce $\tau \in (0, 2\pi)$ as a dimensionless Lagrangian azimuthal co-ordinate on the tube wall. Assuming that the tube wall is linearly elastic with Young's modulus E and Poisson ratio ν, we define the extensional stiffness D and bending stiffness K respectively as

$$D = \frac{Ed}{1-\nu^2}, \qquad K = \frac{Ed^3}{12(1-\nu^2)}. \tag{2.1}$$

We suppose that changes to the deformation of the tube wall occur over a typical time scale T, and are induced by an applied transmural pressure $p^*_{\text{tm}}(\tau, z, t)$, with dimensional scale $\mathscr{P}$. For simplicity, we assume that the transmural pressure is even and π-periodic in τ. This corresponds to mirror symmetry in the x and y axes.

We introduce the dimensionless transmural pressure as

$$\tilde{P}(\tau, z, t) = \frac{p^*_{\text{tm}}(\tau, z, t)}{\mathscr{P}}. \tag{2.2}$$

2.2 *Dimensionless parameters and asymptotic regime*

We will work within an asymptotic regime in which the tube is long and the wall is thin. Defining dimensionless parameters ℓ and δ for the respective aspect ratios, we have

$$\ell = \frac{L}{a} \gg 1, \quad \text{and} \quad \delta = \frac{d}{a} \ll 1. \tag{2.3}$$

Whittaker *et al.* (**10**) showed that the dominant mechanisms that balance the transmural pressure (at leading-order) within this regime are those of azimuthal bending and/or the action of axial tension through axial curvature. For the case of Walters *et al.* (**12**) the pressure may also be balanced by contributions due to wall inertia. To describe the relative

magnitudes of the transmural pressure scale $\mathscr{P}$, the bending stiffness K, the axial tension F, and the mass m, we introduce the dimensionless parameters:

$$\tilde{F} = \frac{aF}{2\pi K\ell^2} = O(1), \qquad M = \frac{ma^4}{KT^2} \lesssim 1, \qquad \epsilon = \frac{a^3\mathscr{P}}{K} \ll 1. \tag{2.4}$$

The parameter $\tilde{F}$ gives the ratio between axial tension–curvature effects and azimuthal bending, and can be though of as a dimensionless axial tension. The parameter M gives the ratio between wall inertia and azimuthal bending and can be thought of as a dimensionless mass. Taking $\tilde{F} = O(1)$ and $M \lesssim O(1)$ enables effects due to axial tension–curvature, wall inertia and azimuthal bending all to be present at leading-order. The parameter ϵ is the ratio of the pressure forcing to the resistance from azimuthal bending. It gives an estimate of the dimensionless amplitude of the deformations (ϵa in dimensional terms). Taking $\epsilon \ll 1$ ensures that we have small amplitude deformations, and that we can linearise the problem about the base state.

Using the set-up of Whittaker *et al.* (**10**), we consider an asymptotic solution that is zeroth order in δ, ℓ^{-1}, and first order in ϵ. There is one constraint on the relative magnitudes of δ and ℓ^{-1}, which ensures that boundary layers in the axial co-ordinate (containing unwanted shear affects) are passive, and have negligible affect on the bulk solution. We refer readers to (**13**) and (**14**) for a comprehensive discussion on this topic. Following (**13**) and (**14**), we introduce the dimensionless parameter

$$\mathscr{F} = \frac{\tilde{F}\delta^2\ell^2}{12(1-\nu^2)} \tag{2.5}$$

to characterize boundary layer thickness for the asymptotic regimes considered here. For $\mathscr{F} \gg 1$, an axial boundary layer of dimensional thickness $O(a\delta\ell)$ is present, which is necessarily passive when $\delta \ll 1$. On the other hand, when $\mathscr{F} \ll 1$, an outer shear layer of dimensional thickness $O(a\mathscr{F}^{-1/2})$ is present. For this layer to have negligible affect on the bulk solution, we require $a\mathscr{F}^{-1/2} \ll L$. Overall, this amounts to the constraint

$$\delta\ell^2 \gg 1. \tag{2.6}$$

2.3 *Description of the tube wall and deformation*

The tube's cross-section is initially elliptical. We introduce the constant ellipticity parameter σ_0 such that the tube's semi-major and semi-minor axes are of length $ac\cosh\sigma_0$ and $ac\sinh\sigma_0$ respectively. The normalisation factor $c(\sigma_0)$ is chosen to set the initial circumference of the tube's cross-section to be $2\pi a$. It is found that c is given by

$$c = \frac{\pi\,\mathrm{sech}(\sigma_0)}{2E(\mathrm{sech}(\sigma_0))}, \tag{2.7}$$

where $E(k) = \int_0^{\pi/2}\sqrt{1-k^2\sin^2\theta}\mathrm{d}\theta$ is the complete elliptic integral of the second kind.

The tube wall's midplane is parametrised by the dimensionless co-ordinates $\tau \in (0, 2\pi)$ and $z \in (0, 1)$. As depicted in Fig. 4, the azimuthal co-ordinate τ varies along the circumference of the tube's cross-section, and z is the distance along the tube's central

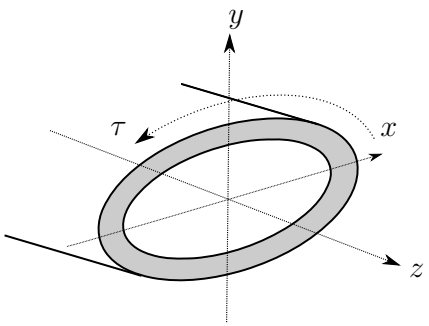

Figure 4: Schematic of a shell segment illustrating the dimensionless co-ordinate system (τ, z). Here τ is the azimuthal co-ordinate oriented around the circumference of the tube's cross-section. The co-ordinate z represents the distance along the tube's central axis.

axis. In its undeformed configuration, the position vector of the tube wall is given explicitly by

$$\bar{\boldsymbol{r}}(\tau, z) = a \begin{pmatrix} c\cosh(\sigma_0)\cos(\tau) \\ c\sinh(\sigma_0)\sin(\tau) \\ \ell z \end{pmatrix}. \tag{2.8}$$

We define unit vectors $\hat{\boldsymbol{t}}, \hat{\boldsymbol{z}}$ and $\hat{\boldsymbol{n}}$, which are oriented in the azimuthal, axial and normal directions respectively. They are given explicitly by

$$\hat{\boldsymbol{t}} = \frac{c}{h}\begin{pmatrix} -\cosh(\sigma_0)\sin(\tau) \\ \sinh(\sigma_0)\cos(\tau) \\ 0 \end{pmatrix}, \qquad \hat{\boldsymbol{z}} = \begin{pmatrix} 0 \\ 0 \\ 1 \end{pmatrix}, \qquad \hat{\boldsymbol{n}} = \frac{c}{h}\begin{pmatrix} \sinh(\sigma_0)\cos(\tau) \\ \cosh(\sigma_0)\sin(\tau) \\ 0 \end{pmatrix}, \tag{2.9}$$

where

$$h(\tau) = c\left(\frac{1}{2}\cosh(2\sigma_0) - \frac{1}{2}\cos(2\tau)\right)^{\frac{1}{2}} > 0 \tag{2.10}$$

is the dimensionless scale factor for the elliptical co-ordinate system.

By using (2.8)–(2.9), we find that the undisturbed cross-sectional area $\bar{A}$ and the base-state azimuthal curvature $\bar{B}(\tau)$ of the undeformed tube are given respectively by

$$\bar{A} = \pi a^2 \frac{c^2\sinh(2\sigma_0)}{2}, \qquad \bar{B}(\tau) = \hat{\boldsymbol{n}}\cdot\frac{1}{h}\frac{\mathrm{d}\hat{\boldsymbol{t}}}{\mathrm{d}\tau} = -\frac{c^2\sinh(2\sigma_0)}{2h^3}. \tag{2.11}$$

Throughout this paper we shall refer to a set of six representative values of σ_0, $(s_0, s_1, s_2, s_3, s_4, s_5)$ which are presented in table 1. Fig. 5 shows the corresponding elliptical cross-sections.

We now introduce variables to describe the deformation of the tube from its undeformed configuration. We follow Whittaker *et al.* (**10**) who used the four deformation functions: $\xi(\tau, z, t), \eta(\tau, z, t), \zeta(\tau, z, t)$ and $\zeta_a(z, t)$. The deformed position of the part of the tube wall

j	0	1	2	3	4	5
$\sqrt{\bar{A}(s_j) - \bar{A}(s_0)}$	0	γ	2γ	3γ	4γ	5γ
s_j	∞	0.9540	0.6000	0.3840	0.2194	0.0755

Table 1: The representative eccentricity parameter values s_j of σ_0. The values were chosen such that $\sqrt{\bar{A}(s_j) - \bar{A}(s_0)} = \gamma j$ is linear in j, where $\gamma = \frac{1}{2}\sqrt{\bar{A}(0.6) - \bar{A}(s_0)}$ is chosen such that $s_2 = 0.6$ for a comparison with the study of Whittaker *et al.* (**10**). The resulting elliptical cross-sections are shown in Fig. 5. The s_j values were deduced numerically using the built in `Matlab` function `fzero`.

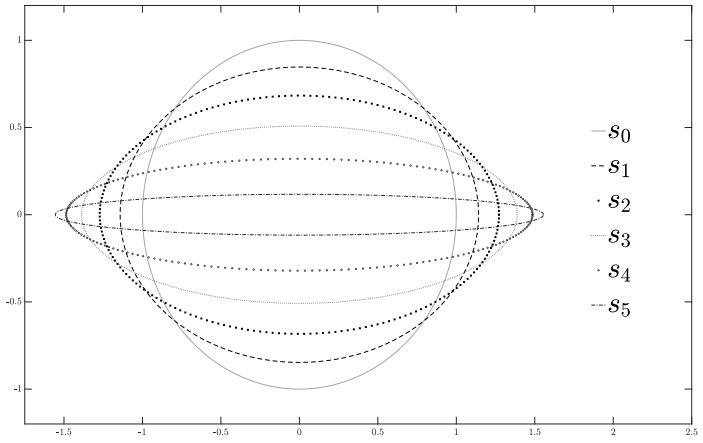

Figure 5: The elliptical cross-sections for $\sigma_0 \in \{s_0, s_1, s_2, \ldots, s_5\}$ as given in table 1. The curves are plotted using (2.7) and (2.8) with $a = 1$.

which was at $\bar{\mathbf{r}}(\tau, z)$ in the undeformed configuration is then given by

$$\boldsymbol{r}(\tau, z, t) = \bar{\boldsymbol{r}}(\tau, z) + \frac{\epsilon a}{h(\tau)}\left(\xi(\tau, z, t)\hat{\boldsymbol{n}} + \eta(\tau, z, t)\hat{\boldsymbol{t}}\right) + \epsilon a \ell \left(\frac{1}{\ell^2}\zeta(\tau, z, t) + \delta^2 \zeta_a(z, t)\right)\hat{\boldsymbol{z}}. \quad (2.12)$$

The function $\xi(\tau, z, t)$ describes the component of displacement normal to the tube wall, $\eta(\tau, z, t)$ describes the displacement in the azimuthal direction, and the functions $\zeta(\tau, z, t)$ and $\zeta_a(z, t)$ represent the axial displacements. The two functions are used here to distinguish between the azimuthal-mean axial displacement $\zeta_a(z, t)$, and the azimuthally varying component $\zeta(\tau, z, t)$, which have different scales. The pre-factors present in (2.12) ensure that the dimensional scales are consistent whilst rendering the deformation functions $\xi, \eta, \zeta, \zeta_a$ all $O(1)$.

Whittaker *et al.* (**10**) argued that at leading-order there is negligible azimuthal stretching and that the in-plane shear is uniform within each cross-section. They showed that these

physical constraints result in the following relationships between the displacement functions:

$$\xi \sinh(2\sigma_0) + \frac{2h^2}{c^2}\frac{\partial \eta}{\partial \tau} - \eta \sin(2\tau) = 0, \tag{2.13}$$

$$\frac{\partial \eta}{\partial z} + \frac{\partial \zeta}{\partial \tau} = \frac{h(\tau)}{2\pi}\frac{\mathrm{d}}{\mathrm{d}z}\int_0^{2\pi} \eta \,\mathrm{d}\tau. \tag{2.14}$$

2.4 *The governing equation for the azimuthal displacements*

Whittaker *et al.* (**10**) obtained a single governing equation for η in the case where wall inertia is neglected and the transmural pressure is azimuthally uniform. This was later extended by Walters *et al.* (**12**) to include the inertia of the tube wall.

The derivation of the governing equation by Whittaker *et al.* (**10**) and Walters *et al.* (**12**) starts with linear constitutive laws (**15**) for the elastic wall and the Kirchoff–Love shell equations (**16**). On substituting the deformation (2.12) into these equations and neglecting terms of $O(\epsilon, \ell^{-1}, \delta)$, a set of three equations of motion in the normal, azimuthal and axial directions is obtained. The unknowns in these equations are displacement functions $\xi, \eta, \zeta, \zeta_a$ and a hoop stress $\tilde{N}$ (the latter is effectively a Lagrange multiplier for the constraint of no azimuthal stretching).

The constraints (2.13)–(2.14) are then used to eliminate ξ and ζ from the system in favour of η. The hoop stress $\tilde{N}$ is then eliminated between the normal and azimuthal equations. Since neither involve ζ_a, a single partial integro-differential equation for η is thus obtained. Once a solution for η has been found, the other displacement functions ξ, ζ and ζ_a can be recovered using (2.13), (2.14), and the axial equation respectively.

In the present work, we replicate this procedure, but allow for azimuthal variation in the transmural pressure $\tilde{P}(\tau, z, t)$. The details are omitted for brevity, but we obtain the following governing equation for η:

$$\hat{\mathscr{L}}(\hat{\mathscr{K}}(\eta)) - h\frac{\partial^2}{\partial z^2}\hat{\mathscr{R}}(\eta) - \tilde{F}\frac{\partial^2}{\partial z^2}\hat{\mathscr{J}}(\eta) + M\frac{\partial^2}{\partial t^2}\hat{\mathscr{J}}(\eta) = -\tanh^2 2\sigma_0 \frac{\partial}{\partial \tau}\left(\frac{\tilde{P}(\tau, z, t)}{\bar{B}(\tau)}\right), \tag{2.15}$$

where the linear differential operators $\hat{\mathscr{L}}, \hat{\mathscr{K}}$ and $\hat{\mathscr{J}}$, are given explicitly by

$$\hat{\mathscr{L}}(\eta) = \tanh(2\sigma_0)\left(-\bar{B}\frac{\partial}{\partial \tau}\left(\frac{\eta}{h}\right) - \frac{\partial}{\partial \tau}\left(\frac{1}{\bar{B}h}\frac{\partial}{\partial \tau}\left(\frac{1}{h}\frac{\partial}{\partial \tau}\left(\frac{\eta}{h}\right)\right)\right)\right), \tag{2.16}$$

$$\hat{\mathscr{J}}(\eta) = \tanh^2(2\sigma_0)\left(\eta - \frac{\partial}{\partial \tau}\left(\frac{1}{\bar{B}^2 h}\frac{\partial}{\partial \tau}\left(\frac{\eta}{h}\right)\right)\right), \tag{2.17}$$

$$\hat{\mathscr{K}}(\eta) = \tanh(2\sigma_0)\frac{\partial}{\partial \tau}\left(\frac{\bar{B}\eta}{h} + \frac{1}{h}\frac{\partial}{\partial \tau}\left(\frac{1}{\bar{B}h}\frac{\partial}{\partial \tau}\left(\frac{\eta}{h}\right)\right)\right), \tag{2.18}$$

and the integral operator $\hat{\mathscr{R}}(\eta)$ is defined as

$$\hat{\mathscr{R}}(\eta) = \frac{12(1-\nu)\tanh^2 2\sigma_0}{2\pi\delta^2\ell^2}\int_0^{2\pi} \eta \,\mathrm{d}\tau. \tag{2.19}$$

These operators differ slightly from when they were originally presented by previous

authors due to the inclusion of the linear scaling $\tanh^2 2\sigma_0$. This scaling is introduced to prevent unbounded behaviour in both $\hat{\mathscr{J}}(\eta)$ and the forcing of (2.15) as $\sigma_0 \to 0$, which arises due to the small σ_0 behaviour of the azimuthal curvature

$$\bar{B} \sim -\frac{\sinh(2\sigma_0)}{\pi \sin^3 \tau} \qquad \text{as} \qquad \sigma_0 \to 0. \tag{2.20}$$

Owing to the assumed symmetry of the transmural pressure ($\tilde{P}$ is even and π-periodic), together with the parity of the operators $\hat{\mathscr{L}}\hat{\mathscr{K}}$ and $\hat{\mathscr{J}}$, it follows that the only component of η that is forced by the transmural pressure will be odd and π-periodic. We therefore proceed by seeking solutions for η that are odd and π-periodic. This results in $\hat{\mathscr{R}} \equiv 0$, and the governing equation (2.15) reduces to the PDE

$$\hat{\mathscr{L}}(\hat{\mathscr{K}}(\eta)) - \tilde{F}\frac{\partial^2}{\partial z^2}\hat{\mathscr{J}}(\eta) + M\frac{\partial^2}{\partial t^2}\hat{\mathscr{J}}(\eta) = -\tanh^2 2\sigma_0 \frac{\partial}{\partial \tau}\left(\frac{\tilde{P}(\tau, z, t)}{\bar{B}(\tau)}\right). \tag{2.21}$$

Equation (2.21) is identical to the governing PDE derived by Walters *et al.* (**12**), with the exception of the linear scaling applied to the operators, and the form of the pressure term on the right hand side.

2.5 *Boundary conditions*

There are two sets of boundary conditions associated with the problem (2.21). The first applies at the tube ends $z = 0$ and $z = 1$ and encapsulates the requirement that the elastic tube is pinned to rigid supports. The conditions are given explicitly by

$$\eta = 0 \qquad \text{on} \qquad z = 0, 1. \tag{2.22}$$

The second set of boundary conditions are with respect to the azimuthal co-ordinate τ, and arise due to the symmetries of the problem. The assumption that η is both odd and π periodic in τ means that we can restrict the azimuthal domain to $\tau \in (0, \pi/2)$ and conditions on the continuity of odd derivatives in η are automatically satisfied. The remaining boundary conditions are given by

$$\eta = \frac{\partial^2 \eta}{\partial \tau^2} = \frac{\partial^4 \eta}{\partial \tau^4} = 0 \qquad \text{on} \qquad \tau = 0, \frac{\pi}{2}. \tag{2.23}$$

3. A generalised eigenvalue problem

In this section we introduce a generalised eigenvalue problem whose eigenfunctions will be used to construct a solution to (2.21). We will show that the operators $\hat{\mathscr{L}}\hat{\mathscr{K}}$ and $\hat{\mathscr{J}}$ are self-adjoint, as well as present the fundamental result that the eigenfunctions form a complete set. We compute numerical solutions to the eigenvalue problem at each $\sigma_0 \in \{s_1, s_2, s_3, s_4, s_5\}$, and also obtain an analytical solution in the limit $\sigma_0 \to \infty$.

3.1 *The eigenvalue problem*

The generalised eigenvalue problem for $y(\tau)$ that we need to consider in order to construct solutions to (2.21)–(2.23) is:

$$\hat{\mathscr{L}}\hat{\mathscr{K}}(y) - \lambda \hat{\mathscr{J}}(y) = 0 \qquad \text{for} \qquad \tau \in (0, \pi/2), \tag{3.1}$$

subject to

$$y = \frac{\mathrm{d}^2 y}{\mathrm{d}\tau^2} = \frac{\mathrm{d}^4 y}{\mathrm{d}\tau^4} = 0 \qquad \text{on} \qquad \tau = 0, \frac{\pi}{2}. \tag{3.2}$$

We observe that (3.1) is a 6th-order ordinary differential equation for $y(\tau)$, with one parameter λ (the eigenvalue) and 6 boundary conditions. Since the system is linear and homogeneous, the remining degree of freedom is the normalisation (linear scaling) of the solutions (see below). Let $y = Y_n(\tau)$ be the eigenfunctions of (3.1) with corresponding eigenvalues λ_n, ordered such that $\lambda_1 < \lambda_2 < ....$

3.2 *Self-adjointness of the operators and eigenfunction orthogonality*

We define the inner product

$$\langle u, v \rangle = \int_0^{\pi/2} \frac{1}{h} uv \mathrm{d}\tau. \tag{3.3}$$

From the definitions (2.17)–(2.18) of $\hat{\mathscr{L}}\hat{\mathscr{K}}$ and $\hat{\mathscr{J}}$ we can integrate by parts to show that the operators $\hat{\mathscr{L}}\hat{\mathscr{K}}$ and $\hat{\mathscr{J}}$ are self-adjoint with respect to (3.3). In other words:

$$\langle \hat{\mathscr{L}}\hat{\mathscr{K}}(u), v \rangle = \langle u, \hat{\mathscr{L}}\hat{\mathscr{K}}(v) \rangle \qquad \text{and} \qquad \langle \hat{\mathscr{J}}(u), v \rangle = \langle u, \hat{\mathscr{J}}(v) \rangle \tag{3.4}$$

for all smooth functions u and v that satisfy (3.2).

Using the relationships (3.4), together with the eigenvalue equation (3.1), we can employ the usual method to show that the eigenfunctions satisfy the orthogonality relation

$$\langle Y_n, \hat{\mathscr{J}}(Y_m) \rangle = 0 \qquad \text{for} \qquad n \neq m. \tag{3.5}$$

The individual eigenfunctions Y_n are not orthogonal to one another. Moreover, it can also be shown that the bilinear form $\langle u, \hat{\mathscr{J}}(v) \rangle$ is positive definite on $(0, \pi/2)$, since, after integrating by parts recursively

$$\langle u, \hat{\mathscr{J}}(u) \rangle = \tanh^2(2\sigma_0) \int_0^{\pi/2} \left(\frac{1}{h}|u|^2 + \frac{1}{(\bar{B})^2 h} \left| \frac{\partial}{\partial \tau} \left(\frac{u}{h} \right) \right|^2 \right) \mathrm{d}\tau \geqslant 0, \tag{3.6}$$

with equality if and only if $u \equiv 0$. We therefore define the normalisation condition

$$\langle Y_n, \hat{\mathscr{J}}(Y_n) \rangle \equiv \int_0^{\pi/2} \frac{1}{h} Y_n \hat{\mathscr{J}}(Y_n) \mathrm{d}\tau = 1, \tag{3.7}$$

which sets the amplitude of the eigenfunctions. This condition, together with the orthogonality result (3.5) yields the property

$$\langle Y_n, \hat{\mathscr{J}}(Y_m) \rangle = \delta_{nm}, \tag{3.8}$$

where δ_{nm} is the Kronecker delta.

It can be shown that the set of eigenfunctions $\{Y_n\}$ form a *complete set*, in the sense that any smooth function satisfying the boundary conditions (3.2) can be represented as a linear combination of the eigenfunctions Y_n. The result is obtained by defining appropriate function spaces and equipping them with carefully chosen inner products such that theorem 6.3.1 in Blanchard and Brüning (**17**) yields a basis of eigenfunctions that satisfy (3.1)–(3.2). We omit the details here for brevity, however the full proof can be found in the PhD thesis of Netherwood (**18**).

3.3 *The circular limit $\sigma_0 \to \infty$*

For general σ_0, the system (3.1), (3.2) and (3.7) can only be solved numerically. However, analytic results can be obtained in the limit $\sigma_0 \to \infty$, which corresponds to the tube's initial cross-section becoming circular. These results are then used to formulate an initial guess when solving the problem numerically for general σ_0 in §3.4. The analytical results can also be used as a check of the numerical solutions.

It is simple to show that in the limit as $\sigma_0 \to \infty$, we have $\bar{B} \to -1$ and $h \to 1$. It follows that in this circular limit, the eigenvalue problem (3.1) reduces to

$$\frac{\mathrm{d}^6 Y_n}{\mathrm{d}\tau^6} + 2\frac{\mathrm{d}^4 Y_n}{\mathrm{d}\tau^4} + (1-\lambda_n)\frac{\mathrm{d}^2 Y_n}{\mathrm{d}\tau^2} + \lambda_n Y_n = 0, \tag{3.9}$$

subject to

$$Y_n = \frac{\mathrm{d}^2 Y_n}{\mathrm{d}\tau^2} = \frac{\mathrm{d}^4 Y_n}{\mathrm{d}\tau^4} = 0 \qquad \text{on} \qquad \tau = 0, \frac{\pi}{2}. \tag{3.10}$$

The normalisation condition (3.7) becomes

$$\int_0^{\pi/2} Y_n^2 + \left(\frac{\mathrm{d}Y_n}{\mathrm{d}\tau}\right)^2 \mathrm{d}\tau = 1, \tag{3.11}$$

after applying integration by parts.

The ordinary differential equation (3.9) has constant coefficients and contains only even derivatives of τ. This observation, together with the periodicity implied by the boundary conditions (3.2), suggests we should seek solutions of the form

$$Y_n = D_n \sin(2n\tau) \;\text{ for }\; n \in \mathbb{N}, \tag{3.12}$$

where the constants D_n are set by the normalisation (3.11). By substituting (3.12) into (3.9) and arranging for λ_n we find that

$$\lambda_n = \frac{64n^6 - 32n^4 + 4n^2}{1 + 4n^2}. \tag{3.13}$$

Finally, the normalisation condition (3.11) yields D_n, and hence the solution

$$Y_n(\tau) = \frac{2}{\sqrt{\pi(1+4n^2)}} \sin(2n\tau). \tag{3.14}$$

Plots of the eigenfunctions (3.14) are shown in Fig. 6.

3.4 *Numerical method for general σ_0*

The eigenvalue problem (3.1)–(3.2) and (3.7) with $y = Y_n(\tau)$ was solved numerically by using the built in `Matlab` solver `bvp4c`. The solver requires that we write the governing equation as a first-order coupled system of ODEs. We do this in the standard way by using Y_n and its first five derivatives as the variables.

For the normalisation, the eigenfunctions were initially normalised subject to $Y_n'(0) = 1$, since this was numerically more convenient than using the integral condition (3.7) when

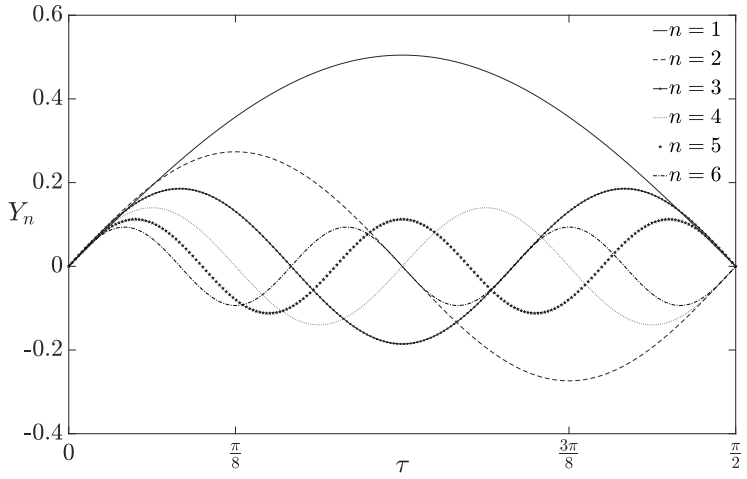

Figure 6: Plots of the eigenfunctions Y_n for modes $n = 1, 2, ..., 6$ in the limit as $\sigma_0 \to \infty$, corresponding to analytically obtained solutions (3.14) of the system (3.9)–(3.11).

calling the solver. Once a numerical solution of (3.1)–(3.2) has been found, it is scaled to satisfy the required normalisation (3.7).

The solver `bvp4c` requires an initial guess for the solution and any parameters (the eigenvalue in this case). Initially, when considering an approximation for the eigenfunctions of (3.1)–(3.2), it seemed that the analytical results for $\sigma_0 \to \infty$ studied in §3.3 would provide a sufficient approximation for all σ_0. However, within this regime the method would sometimes (and unpredictably) converge to different solutions (corresponding to different modes), particularly at smaller σ_0. Therefore, in order to obtain a reliable solution for the nth mode at each σ_0, we iterated through descending values of σ_0 and used each preceding solution as the initial approximation $\tilde{y}$ of the eigenfunction at the next value of σ_0. In order to provide an initial estimate $\tilde{\lambda}_n$ of the eigenvalue, we calculated the Rayleigh quotient for each σ_0 using our eigenfunction estimate:

$$\tilde{\lambda}_n = \frac{\langle \tilde{y}, \hat{\mathscr{L}}\hat{\mathscr{K}}(\tilde{y})\rangle}{\langle \tilde{y}, \hat{\mathscr{J}}(\tilde{y})\rangle}. \tag{3.15}$$

For each n and σ_0, once the approximations $\tilde{y}_n$ and $\tilde{\lambda}_n$ had been determined, we called `bvp4c` on an initial mesh of 500 points on the interval $\tau \in (0, \pi/2)$, which found a numerical approximation of the system. Each solution y_n from `bvp4c` then needed to be scaled to satisfy the normalisation condition (3.7). The inner product

$$\begin{aligned} \gamma_n &= \langle y_n, \hat{\mathscr{J}}(y_n)\rangle, \\ &= \int_0^{\pi/2} \frac{1}{h} y_n \cdot \hat{\mathscr{J}}(y_n)\, \mathrm{d}\tau, \end{aligned} \tag{3.16}$$

was evaluated numerically. Once γ_n had been found, the normalised eigenfunction was

σ_0	λ_1	λ_2	λ_3	λ_4	λ_5	λ_6
$s_0 = \infty$	7.20000	211.765	1191.89	3907.94	9703.96	20308.0
$s_1 = 0.9540$	6.97182	207.340	1180.73	3887.93	9672.74	20263.1
$s_2 = 0.6$	6.42638	194.436	1140.73	3811.43	9552.18	20090.5
$s_3 = 0.3840$	5.83285	176.578	1066.20	3636.83	9240.97	19614.3
$s_4 = 0.2194$	5.38682	160.336	979.575	3384.11	8695.61	18631.7
$s_5 = 0.0755$	5.16604	151.227	922.705	3191.48	8217.27	17647.5

Table 2: Numerical results for the eigenvalues λ_n of (3.1)–(3.2). The eigenvalues are shown for the first six modes and are calculated numerically at each $\sigma_0 \in \{s_0, s_1, s_2, s_3, s_4, s_5\}$. The row corresponding to $s_0 = \infty$ contains values for the eigenvalues in the limit $\sigma_0 \to \infty$ from (3.13).

computed as

$$Y_n(\tau) = \frac{1}{\sqrt{\gamma_n}} y_n(\tau). \tag{3.17}$$

3.5 *Numerical results for the eigenvalue problem*

In Fig. 7 we plot the normalised eigenfunctions $Y_n(\tau)$ for modes $n = 1, 2, ..., 6$ that satisfy (3.1), (3.2) and (3.7) for ellipticity parameter $\sigma_0 \in \{s_0, s_1, s_2, ..., s_5\}$ (see table 1). It can be seen that the number of half-oscillations of each eigenfunction present on the interval $(0, \pi/2)$ is equal to the mode number n. Moreover, we observe that for decreasing values of σ_0 relative to the $\sigma_0 = \infty$ case, the corresponding eigenfunctions are increasingly out of phase (to the right) with the analytic limits $Y_n \propto \sin(2n\tau)$. The amplitude of the eigenfunctions is found to be larger towards the $\tau = 0$ end of the azimuthal domain.

Fig. 8 shows the eigenvalues λ_n (scaled by their circular limit behaviour (3.13)) plotted against σ_0 for modes $n = 1, 2, ..., 6$. We observe that, for each n, the plots maintain a similar-shaped profile. However, there are large differences in the magnitude of λ_n (see table 2) as we change the mode number, n. Fig. 8 also shows that the numerically obtained eigenvalues λ_n converge to the analytically obtained limits (3.13) as $\sigma_0 \to \infty$.

4. Solution by series expansions

In this section we seek a full series solution to (2.21)–(2.23). We represent the solution as a sum over the eigenfunctions studied in §3.1, and show that this allows us to fully decompose the governing equation (2.21) into a system of uncoupled linear partial differential equations with constant coefficients.

4.1 *Decomposition of $\eta(\tau, z, t)$*

Let $\eta(\tau, z, t)$ be the solution of (2.21)–(2.23). We assume on physical grounds that such a solution will exist. Recall the inner product (3.3) and define

$$a_n(z, t) = \langle \eta, \hat{\mathscr{J}}(Y_n) \rangle = \int_0^{\pi/2} \frac{1}{h} \eta \hat{\mathscr{J}}(Y_n(\tau)) \, \mathrm{d}\tau. \tag{4.1}$$

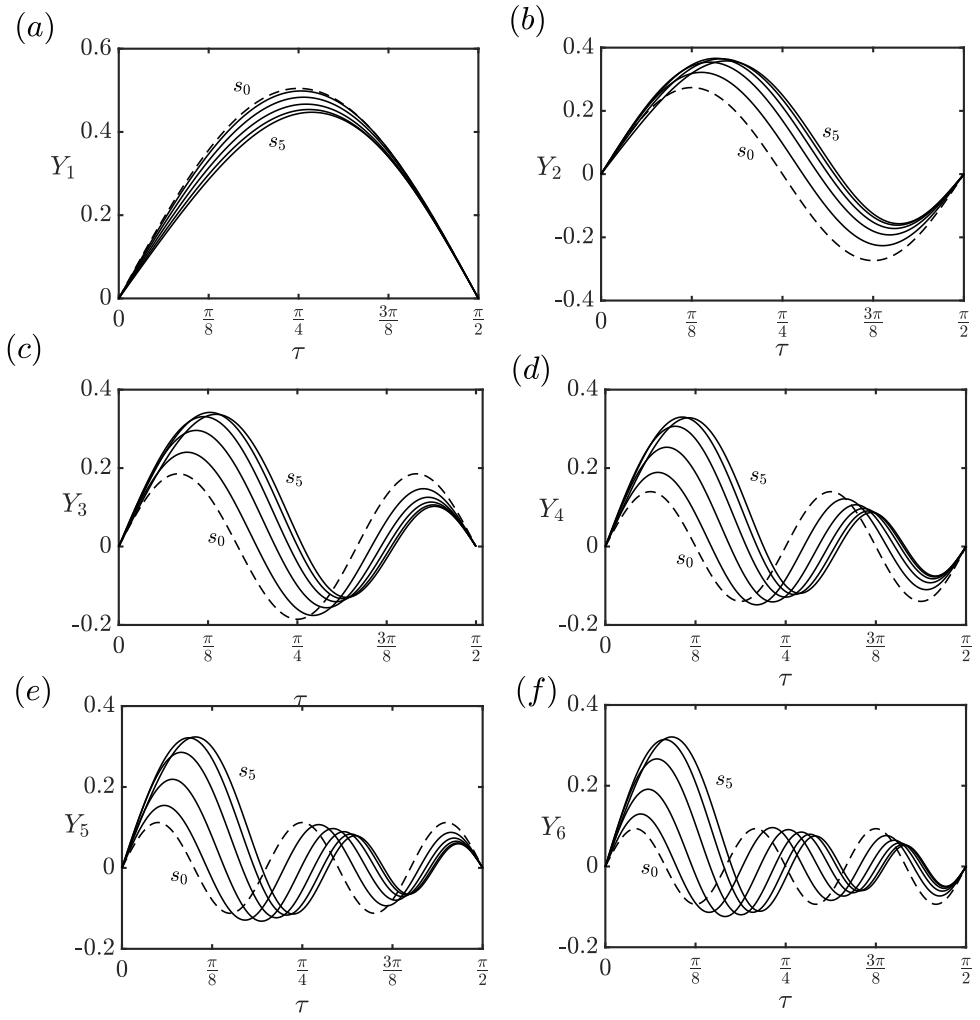

Figure 7: Numerical solutions to the system (3.1), (3.2) and (3.7) for $y = Y_n(\tau)$ (the eigenfunctions) for modes $n = 1, 2, \cdots, 6$ with $\sigma_0 \in \{s_0, s_1, s_2, s_3, s_4, s_5\}$. The dashed curves represent the analytic solution (3.14) obtained in the limit $\sigma_0 \to \infty$.

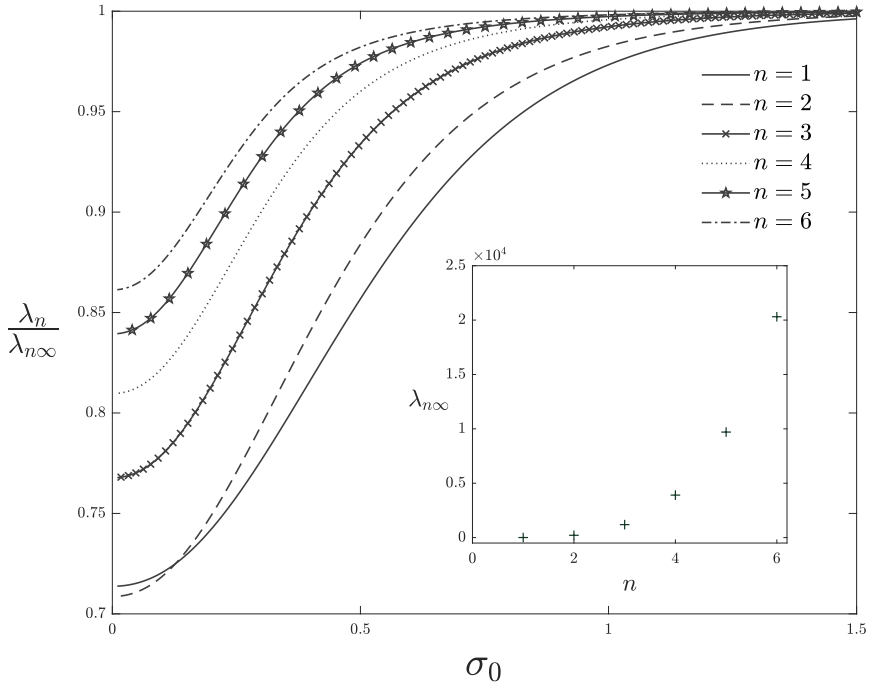

Figure 8: Numerical solutions for the eigenvalues λ_n, plotted against eccentricity parameter σ_0 for modes $n = 1, 2, ..., 6$. Each eigenvalue λ_n has been scaled by its value $\lambda_{n\infty}$ in the circular limit ($\sigma \to \infty$), as given analytically in (3.13). In the inset we plot the circular limit eigenvalues $\lambda_{n\infty}$ against n to give an indication of the relative sizes of the eigenvalues corresponding to different azimuthal modes.

Owing to the completeness of the eigenfunctions Y_n (see §3.2) and the orthogonality relation (3.8), we can express $\eta(\tau, z, t)$ as

$$\eta(\tau, z, t) = \sum_{n=1}^{\infty} a_n(z, t) Y_n(\tau). \tag{4.2}$$

The boundary conditions on $a_n(z, t)$ can then be derived from the pinned-end conditions (2.22), we find that

$$a_n = 0 \qquad \text{on} \qquad z = 0, 1. \tag{4.3}$$

We now take the the inner product of (2.21) with Y_n to obtain

$$\langle \hat{\mathscr{L}}\hat{\mathscr{K}}(\eta), Y_n \rangle - \tilde{F}\frac{\partial^2}{\partial z^2}\langle \hat{\mathscr{J}}(\eta), Y_n \rangle + M\frac{\partial^2}{\partial t^2}\langle \hat{\mathscr{J}}(\eta), Y_n \rangle = Q_n(z, t), \tag{4.4}$$

where

$$Q_n(z,t) = -\tanh^2(2\sigma_0)\int_0^{\pi/2}\frac{1}{h}\frac{\partial}{\partial\tau}\left(\frac{\tilde{P}(\tau,z,t)}{\bar{B}(\tau)}\right)Y_n(\tau)\,\mathrm{d}\tau. \tag{4.5}$$

For the case in which the pressure is azimuthally uniform†, we can write

$$Q_n(z,t) = \tilde{P}(z,t)q_n, \tag{4.6}$$

where

$$q_n = \tanh^2(2\sigma_0)\int_0^{\pi/2} C_P(\tau)Y_n(\tau)\,\mathrm{d}\tau, \tag{4.7}$$

and

$$C_P(\tau) = \frac{3\sin 2\tau}{\sinh 2\sigma_0}. \tag{4.8}$$

Since $\hat{\mathscr{L}}\hat{\mathscr{K}}$ is self-adjoint with respect to (3.3) on the space of functions that satisfy (3.2), and because Y_n is an eigenfunction of (3.1), we have

$$\langle\hat{\mathscr{L}}\hat{\mathscr{K}}(\eta), Y_n\rangle = \langle\eta, \hat{\mathscr{L}}\hat{\mathscr{K}}(Y_n)\rangle = \lambda_n\langle\eta, \hat{\mathscr{J}}(Y_n)\rangle. \tag{4.9}$$

Since $\hat{\mathscr{J}}$ is also self-adjoint, (4.4) becomes

$$\lambda_n\langle\eta, \hat{\mathscr{J}}(Y_n)\rangle - \tilde{F}\frac{\partial^2}{\partial z^2}\langle\eta, \hat{\mathscr{J}}(Y_n)\rangle + M\frac{\partial^2}{\partial t^2}\langle\eta, \hat{\mathscr{J}}(Y_n)\rangle = Q_n(z,t) \tag{4.10}$$

Recalling the definition of $a_n(z,t)$ in (4.1), we obtain:

$$\lambda_n a_n - \tilde{F}\frac{\partial^2 a_n}{\partial z^2} + M\frac{\partial^2 a_n}{\partial t^2} = Q_n(z,t), \quad \text{for } n = 1,2,3,\cdots. \tag{4.11}$$

Equation (4.11) is an uncoupled system of partial differential equations for the axial modes $a_n(z,t)$, forced by $Q_n(z,t)$. We interpret Q_n as the contribution from the pressure to the nth eigenmode. For a given transmural pressure $\tilde{P}$, we can obtain Q_n (via (4.5)) using the numerical solutions for the eigenfunctions $Y_n(\tau)$. Equation (4.11) can then be solved for $a_n(z,t)$ for each n subject to the boundary conditions given by (4.3). Once the modes $a_n(z,t)$ are known, the solution for η is then given by (4.2).

4.2 *Contribution to the area change*

A tube-law provides a relation between the transmural pressure and the tubes cross-sectional area. In place of a single such equation here, we instead obtain a set of equations for the contribution to the area change from each of the azimuthal eigenmodes.

Whittaker *et al.* (**10**) showed that at leading-order, the area change of the tube's cross section is given by

$$A - \bar{A} = \epsilon a^2\int_0^{2\pi}\xi(\tau,z,t)\mathrm{d}\tau + O(\epsilon^2). \tag{4.12}$$

† This case is applicable for the models derived by Whittaker *et al.* (**19**), Whittaker *et al.* (**20**) and Whittaker *et al.* (**21**)

By using (2.13) we can eliminate ξ from (4.12) to obtain

$$A - \bar{A} = \epsilon a^2 \int_0^{2\pi} \left(\frac{\sin 2\tau}{\sinh(2\sigma_0)} \eta - \frac{2h^2}{c^2 \sinh(2\sigma_0)} \frac{\partial \eta}{\partial \tau} \right) \mathrm{d}\tau + O(\epsilon^2). \tag{4.13}$$

Using the symmetry of η, we can restrict the range of integration to $(0, \pi/2)$ and multiply the result by 4. Noting that $2h^2/c^2 = \cosh(2\sigma_0) - \cos(2\tau)$, and that $\eta = 0$ at $\tau = 0, \pi/2$, we can use integration by parts to simplify the second term in the integrand. We obtain:

$$A - \bar{A} = \frac{12\epsilon a^2}{\sinh(2\sigma_0)} \int_0^{\frac{\pi}{2}} \sin(2\tau)\, \eta(\tau, z, t)\, \mathrm{d}\tau + O(\epsilon^2). \tag{4.14}$$

Decomposing $\eta(\tau, z, t)$ as in (4.2) provides

$$A - \bar{A} = \frac{12\epsilon a^2}{\sinh(2\sigma_0)} \sum_{n=1}^{\infty} a_n(z,t) \int_0^{\frac{\pi}{2}} \sin(2\tau) Y_n(\tau) \mathrm{d}\tau + O(\epsilon^2). \tag{4.15}$$

We define the fractional area change $\epsilon\alpha(z,t)$, such that

$$\epsilon\alpha = \frac{A - \bar{A}}{\bar{A}}. \tag{4.16}$$

Substituting (4.15) into (4.16) and using the expression for $\bar{A}$ in (2.11), we obtain

$$\alpha = \frac{24}{\pi c^2 \sinh^2(2\sigma_0)} \sum_{n=1}^{\infty} a_n(z,t) \int_0^{\pi/2} \sin(2\tau) Y_n(\tau) \mathrm{d}\tau + O(\epsilon). \tag{4.17}$$

We define $\alpha_n(z,t) = a_n(z,t) t_n$, where t_n is given by

$$t_n = \frac{24}{\pi c^2 \sinh^2(2\sigma_0)} \int_0^{\pi/2} \sin(2\tau) Y_n(\tau) \mathrm{d}\tau. \tag{4.18}$$

Then it follows that

$$\alpha(z,t) = \sum_{n=1}^{\infty} \alpha_n(z,t), \tag{4.19}$$

and

$$\eta(\tau, z, t) = \sum_{n=1}^{\infty} \frac{1}{t_n} \alpha_n(z,t) Y_n(\tau). \tag{4.20}$$

We therefore interpret $\alpha_n(z,t)$ as the component of the relative area change corresponding to the nth azimuthal eigenmode. By (4.11) and (4.3), each α_n satisfies the partial differential equation

$$\tilde{F} \frac{\partial^2 \alpha_n}{\partial z^2} - M \frac{\partial^2 \alpha_n}{\partial t^2} - \lambda_n \alpha_n = -Q_n t_n, \tag{4.21}$$

subject to

$$\alpha_n = 0 \qquad \text{on} \qquad z = 0, 1. \tag{4.22}$$

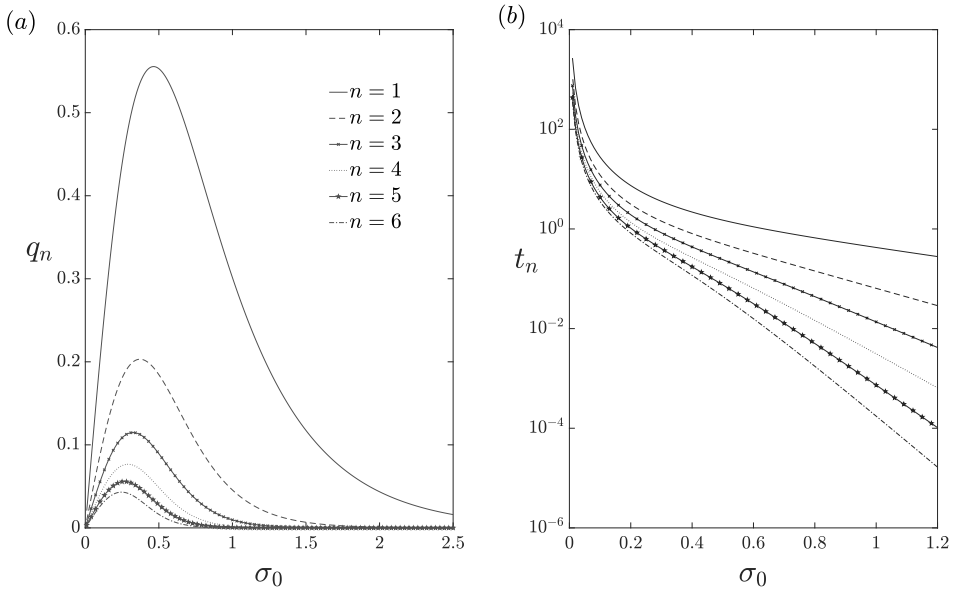

Figure 9: Numerical results for (a) q_n as defined in (4.7), and (b) t_n, as defined in (4.18), plotted as functions of σ_0 for $n = 1, 2, \ldots, 6$. Both plots demonstrate a dominant contribution from the fundamental mode $n = 1$.

Equation (4.21) governs the components α_n, which when summed together, provide the change in cross-sectional area of an initially elliptical elastic-walled tube subject to a given transmural pressure $\tilde{P}(\tau, z, t)$. For simple analytic functions $\tilde{P}(\tau, z, t)$, the system (4.21)–(4.22) can be solved analytically for each n, though the evaluation of Q_n, t_n and λ_n will require numerical attention.

For $\tilde{P}$ uniform in τ, recall that $Q_n = \tilde{P} q_n$, where q_n is given by (4.7). In Fig. 9 we plot q_n and t_n numerically against σ_0 for $n = 1, 2, \ldots, 6$ and observe that in both cases there is a dominant contribution from the first ($n = 1$) mode. We shall term this the fundamental mode. The results demonstrate that a good approximation of the system could be obtained after truncating (4.19) after $n = 1$.

4.3 *Comparison with Whittaker* et al. ***(10)***

In the present notation, the 'tube law' derived by Whittaker *et al.* (**10**) – which applies when the transmural pressure is steady and azimuthally uniform – is given by

$$k_0 \alpha - k_2 \tilde{F} \frac{\mathrm{d}^2 \alpha}{\mathrm{d}z^2} = \tilde{P}(z), \tag{4.23}$$

where k_0 and k_2 are numerically determined constants. If we truncate expansion (4.19) after $n = 1$, and assume a steady deformation in response to a steady azimuthally uniform

σ_0	q_1	q_2	q_3	q_4	q_5	q_6
$s_1 = 0.9540$	0.326229	0.053729	0.012425	0.003104	0.000797	0.000207
$s_2 = 0.6$	0.523926	0.153981	0.065155	0.030600	0.014980	0.007480
$s_3 = 0.3840$	0.540936	0.202923	0.111130	0.069308	0.045950	0.031499
$s_4 = 0.2194$	0.399920	0.167120	0.101920	0.071523	0.053940	0.042484
$s_5 = 0.0755$	0.154760	0.067428	0.042727	0.031198	0.024523	0.020169

Table 3: Results for the numerical constants q_n, as defined in (4.7), which measure the contribution from the (azimuthally uniform) pressure to the nth eigenmode. The values are given for the representative values $\sigma_0 \in \{s_1, s_2, s_3, s_4, s_5\}$. The circular limit case ($\sigma_0 = s_0$) has been omitted since $q_n \to 0$ when $\sigma_0 \to \infty$ for all n as is observed in Fig. 9.

σ_0	t_1	t_2	t_3	t_4	t_5	t_6
$s_1 = 0.9540$	0.468950	0.077235	0.017861	0.004462	0.001146	0.000299
$s_2 = 0.6$	1.104332	0.324563	0.137336	0.064500	0.031576	0.015767
$s_3 = 0.3840$	2.340500	0.878035	0.480852	0.299891	0.198821	0.136295
$s_4 = 0.2194$	6.272272	2.621097	1.598410	1.121761	0.845988	0.6663216
$s_5 = 0.0755$	48.12290	20.9690	13.2861	9.701156	7.62547	6.27148

Table 4: Results for the numerical constants t_n, as defined in (4.18), which measure the effect of the nth modes amplitude on the area change. The values are given for the representative values $\sigma_0 \in \{s_1, s_2, s_3, s_4, s_5\}$.

transmural pressure, then equation (4.21) reduces to

$$\frac{\lambda_1}{q_1 t_1}\alpha_1 - \frac{\tilde{F}}{q_1 t_1}\frac{\mathrm{d}^2\alpha_1}{\mathrm{d}z^2} = \tilde{P}(z). \tag{4.24}$$

This is the same form as (4.23), but with differently computed coefficients.

In Fig. 10 we plot the results of Whittaker *et al.* (**10**) for k_0 and k_2 together with the expressions λ_1/q_1t_1 and $1/q_1t_1$ (scaled by their circular limit behaviour) appropriate for a comparison. We find that better agreement is found for the comparisons involving k_0, although in both cases, we observe that the two solutions converge towards agreement in the limit as $\sigma_0 \to \infty$. The reason for the agreement at large σ_0 is because the eigenfunction expansion (4.2) of η becomes exactly the Fourier expansion used by Whittaker *et al.* (**10**) in this circular limit (see §3.3). Moreover, for both models, the amplitude of the higher-order azimuthal modes become asymptotically smaller than the amplitude of the fundamental mode. This can be justified by considering the ratio

$$\frac{q_n t_n}{q_1 t_1} = \left(\frac{\int_0^{\pi/2} \sin(2\tau) Y_n(\tau)\,\mathrm{d}\tau}{\int_0^{\pi/2} \sin(2\tau) Y_1(\tau)\,\mathrm{d}\tau} \right)^2. \tag{4.25}$$

Hence, using the analytical solution (3.14) for Y_n as $\sigma_0 \to \infty$, it follows (by orthogonality) that

$$\lim_{\sigma_0 \to \infty} \frac{q_n t_n}{q_1 t_1} = 0 \qquad \text{for} \qquad n \geqslant 2. \tag{4.26}$$

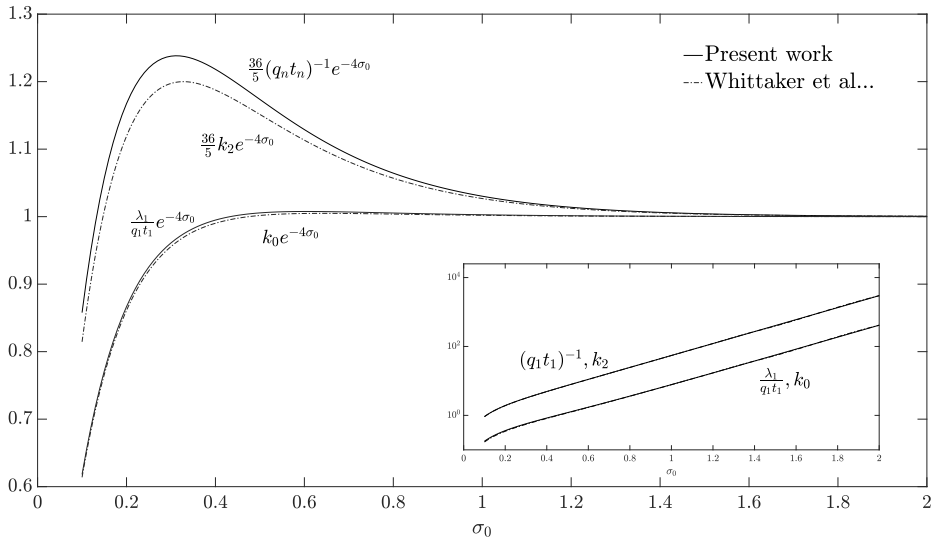

Figure 10: Comparison of the coefficients in the tube-law equations (4.23) and (4.24), as the ellipticity σ_0 is varied. The dot-dashed lines show the values of k_0 and k_2 from Whittaker *et al.* (**10**). The continuous lines show the values of λ_1/q_1t_1 and $1/q_1t_1$ from the present work. In the main figure the values have been scaled by their respective asymptotic forms $e^{4\sigma_0}$ and $5/36e^{4\sigma_0}$ as $\sigma_0 \to \infty$. The raw values are shown in the inset.

5. Application and truncation error estimates

In this section we shall consider the errors incurred by truncating the expansion (4.19); first by constructing general estimates for the magnitude of each α_n, and secondly by considering the specific case of a uniform transmural pressure (for which analytical solutions can be obtained).

5.1 *Estimates of relative area change for steady problems*

We can use (4.21) to obtain estimates for the magnitude of each α_n, which contributes to the relative area change through (4.19). We consider a steady problem in which $\tilde{P} = \tilde{P}(z)$ and $\alpha_n = \alpha_n(z)$. Equation (4.21) then reduces to the ordinary differential equation

$$\tilde{F}\frac{\mathrm{d}^2\alpha_n}{\mathrm{d}z^2} - \lambda_n\alpha_n = -q_n t_n \tilde{P}(z). \tag{5.1}$$

Recall that $z \in (0,1)$ and $\tilde{P}(z) = O(1)$.

When $\tilde{F} \gg \lambda_n$, the second term in (5.1) does not contribute at leading-order. An estimate $\hat{\alpha}_n$ for the magnitude of the relative area change when $\tilde{F} \gg \lambda_n$ is then

$$|\alpha_n(z)| \sim \hat{\alpha}_n = \frac{q_n t_n}{\tilde{F}}. \tag{5.2}$$

Conversely, for $\tilde{F} \ll \lambda_n$, we neglect the first term in (5.1) at leading-order. The estimate

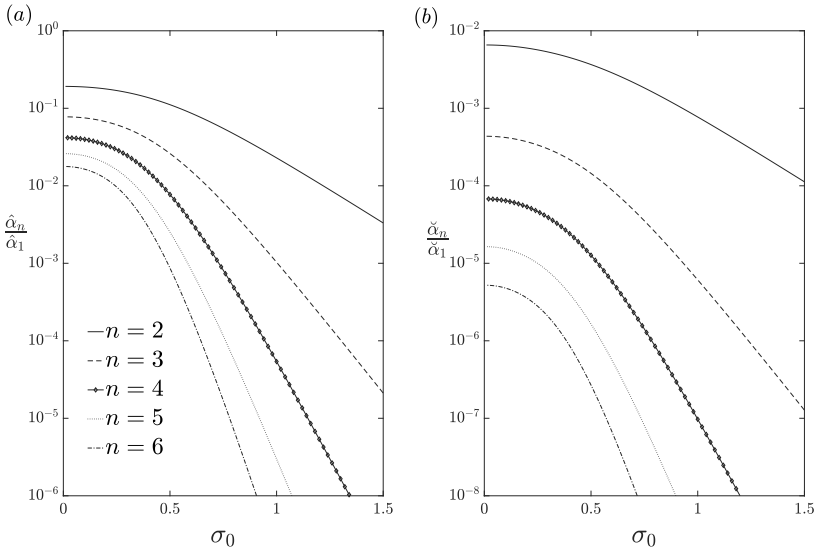

Figure 11: (a) Numerical results for the ratio between the estimates $\hat{\alpha}_n$ for $n = 2, 3, ..., 6$ and the estimate $\hat{\alpha}_1$ from (5.2). (b) Numerical results for the ratio between the estimates $\check{\alpha}_n$ for $n = 2, 3, ..., 6$ and the estimate $\check{\alpha}_1$ from (5.3).

$\check{\alpha}_n$ for the relative area change is then

$$|\alpha_n(z)| \sim \check{\alpha}_n = \frac{q_n t_n}{\lambda_n}. \tag{5.3}$$

Fig. 11 shows the ratios $\hat{\alpha}_n/\hat{\alpha}_1$ and $\check{\alpha}_n/\check{\alpha}_1$ between the higher mode estimates for α_n and the first mode estimate, plotted against σ_0. In both (a) and (b) we see that for smaller σ_0, the higher-order modes provide a more substantial contribution to the relative area change, and become less important as σ_0 becomes larger. Physically, the increase in σ_0 corresponds to the tubes initial cross-section becoming circular. This means that the accuracy in approximating the relative area change of the tube by truncating (4.19) at $n = 1$ depends on the ellipticity of the tubes initial cross-section. For tubes that initially have highly elliptical cross-sections (see Fig. 5), contributions from the higher-order terms in (4.19) may be required.

5.2 *Analytic solution for a steady uniform pressure*

For a steady uniform transmural pressure say $\tilde{P} = -1$, we can solve (4.21)–(4.22) analytically. By using standard methods for solving linear ordinary differential equations with constant coefficients, we find the steady solution

$$\alpha_n(z) = -\frac{q_n t_n}{\lambda_n}\left[1 - \frac{\cosh[\mu_n(z - \frac{1}{2})]}{\cosh\left(\frac{\mu_n}{2}\right)}\right], \tag{5.4}$$

where $\mu_n^2 = \lambda_n/\tilde{F}$.

In Fig. 12 we plot the initial and deformed cross-sectional shapes of the tube located at $z = 0.5$, and in Fig. 13, we plot the solutions (5.4) with $\tilde{P} = -1$ for $\tilde{F} = 1$ and $\tilde{F} = 3$. Comparing with the work of Whittaker *et al.* (**10**) (plotted in Fig. 13) we see that for $n = 1$ and $\sigma_0 = 0.6$ our results are in good agreement.

The solutions (5.4) for α_n have a maximum amplitude at $z = 1/2$, given by

$$\alpha_n\left(\tfrac{1}{2}\right) = -\frac{q_n t_n}{\lambda_n}\left[1 - \operatorname{sech}\left(\frac{\mu_n}{2}\right)\right]. \tag{5.5}$$

When μ_n is large (corresponding to $\tilde{F} \ll \lambda_n$), we see that

$$|\alpha_n(\tfrac{1}{2})| \sim \frac{q_n t_n}{\lambda_n} \qquad \text{for} \qquad \mu_n \gg 1, \tag{5.6}$$

in agreement with the estimate (5.3).

Conversely, for small μ_n ($\tilde{F} \gg \lambda_n$), by making use of the Taylor expansion of $\operatorname{sech}(\mu_n)$, we find that

$$|\alpha_n\left(\tfrac{1}{2}\right)| \sim \frac{q_n t_n}{8\lambda_n}\mu_n^2 \quad \text{for} \quad \mu_n \ll 1. \tag{5.7}$$

Since $\mu_n^2 = \lambda_n/\tilde{F}$, this is consistent with the estimate (5.2).

Figures 14 and 15 show contour plots of the ratios α_2/α_1 and $\alpha_3/(\alpha_1 + \alpha_2)$ evaluated at $z = 0.5$ in $(\tilde{F}, \sigma_0)$ parameter space. The plots provide an understanding of the relative error induced by truncating (4.19) after the first and second modes respectively. Whilst the features of both Fig. 14 and 15 are similar, we find that the retention of the second mode provides an improvement in the error by a factor of between 10^{-1} and $10^{-4.5}$.

The contour plots 14 and 15 show that the relative error induced by truncation decreases monotonically as the ellipticity parameter σ_0 is increased. This observation is in agreement with our analysis in §4.3, where it was shown that the higher order azimuthal modes vanish in the circular limit $\sigma_0 \to \infty$. In both plots we see that smaller values of the axial tension result in a smaller relative error, with the added feature that the error seems to tend towards being independent of $\tilde{F}$ when $\tilde{F}$ is either large or small. To explain these features we consider the dominant contribution α_{n+1}/α_1 to the relative error in truncating (4.19) after the nth mode. Using the estimates (5.2) and (5.3) we find that

$$\frac{\alpha_{n+1}}{\alpha_1} \sim \frac{q_{n+1}t_{n+1}}{q_1 t_1} \qquad \text{for} \qquad \tilde{F} \gg \lambda_n, \tag{5.8}$$

$$\frac{\alpha_{n+1}}{\alpha_1} \sim \frac{\lambda_1}{\lambda_{n+1}}\frac{q_{n+1}t_{n+1}}{q_1 t_1} \qquad \text{for} \qquad \tilde{F} \ll \lambda_n. \tag{5.9}$$

Examining (5.8)–(5.9) we see that both are independent of $\tilde{F}$. Moreover, the presence of the factor λ_1/λ_{n+1} in (5.9) justifies mathematically why the error decreases with an increase in dimensionless axial tension, since $\lambda_{n+1} \ll \lambda_1$ for every n.

6. Conclusions

In this paper we have produced the first formal solution of the problem initially formulated by Whittaker *et al.* (**10**) of the small amplitude deformations of a long thin-walled elastic tube that has an initially axially uniform elliptical cross-section.

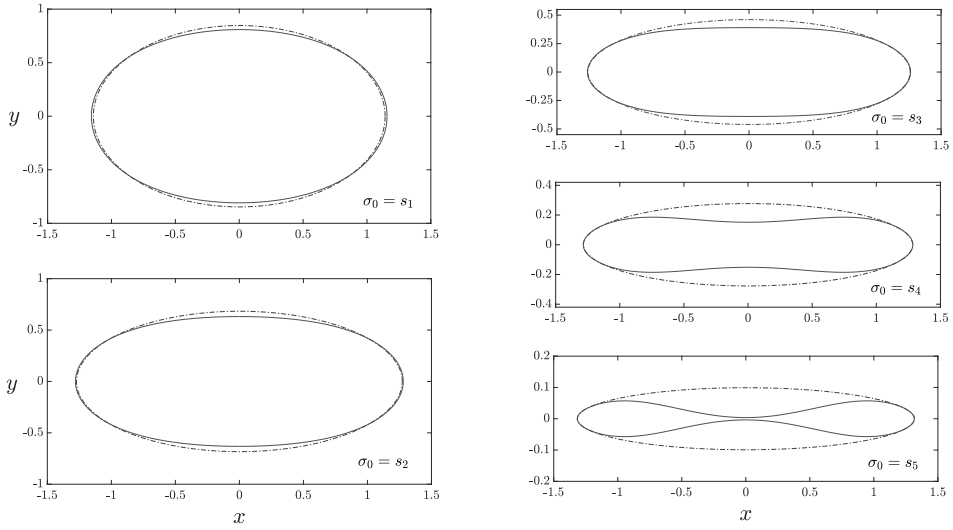

Figure 12: Cross-sectional deformations of an initially elliptical elastic-walled tube induced by a steady uniform transmural pressure for different initial ellipticities. The figure shows the midpoint $z = 1/2$, with the dashed line showing the undeformed and the solid lines showing the deformed wall. All the figures use the same transmural pressure $\tilde{P} \equiv -1$ with $\epsilon = 0.6$, and have the same dimensionless tension $\tilde{F} = 1$. The area changes α_n were calculated using (5.4) and then η was computed from (4.20) and ξ from (2.13). The deformation is then found using (2.12). The expansion (4.19) was truncated after $n = 2$ since adding further modes produced indistinguishable results.

To obtain the solution, we used an eigenfunction expansion method, which involved writing the azimuthal displacement $\eta(\tau, z, t)$ as a sum over the azimuthal eigenfunctions $Y_n(\tau)$ of a generalised eigenvalue problem. This allowed us to derive a series expansion for the tube's dimensionless relative area change α in terms of the dimensionless functions $\alpha_n(z, t)$, which correspond to the area change associated with each azimuthal eigenmode. We showed that the equations for the α_n decouple completely, with each satisfying a PDE

$$\tilde{F}\frac{\partial^2 \alpha_n}{\partial z^2} - M\frac{\partial^2 \alpha_n}{\partial t^2} - \lambda_n \alpha_n = -Q_n t_n, \tag{6.1}$$

where the forcing Q_n from the dimensionless transmural pressure $\tilde{P}$ is given by

$$Q_n(z, t) = -\tanh^2 2\sigma_0 \int_0^{\pi/2} \frac{1}{h}\frac{\partial}{\partial \tau}\left(\frac{\tilde{P}(\tau, z, t)}{\bar{B}(\tau)}\right) \mathrm{d}\tau. \tag{6.2}$$

The coefficients involve the following quantities. In (6.1), $\tilde{F}$ is the dimensionless axial tension, M is the dimensionless inertia coefficient of the tube, λ_n is the eigenvalue of the eigenfunction $Y_n(\tau)$, and t_n is an integral of $Y_n(\tau)$ defined in (4.18). In (6.2), σ_0 defines

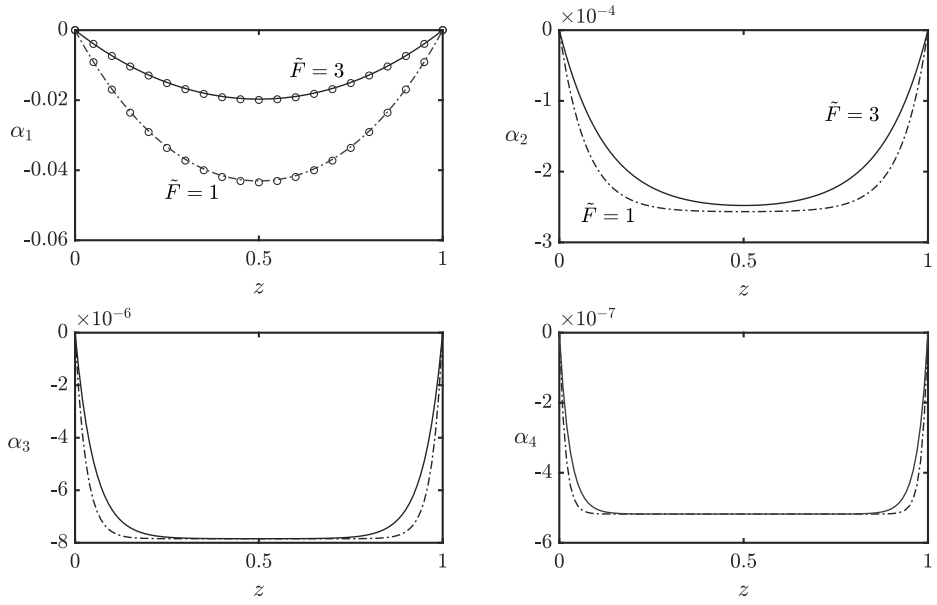

Figure 13: Plots of (5.4) corresponding to solutions of (4.21) for a given transmural pressure $\tilde{P} = -1$ where $\sigma_0 = 0.6$ and $\tilde{F} = 1, 3$. We also plot the results of Whittaker *et al.* (**10**) with the first mode solution using open circles.

the initial ellipticity of the tube, $h(\tau)$ is the dimensionless scale factor for the elliptical coordinates system and $\bar{B}(\tau)$ is the base-state azimuthal curvature. We interpret the terms present on the left hand side of (6.1) as contributions to the amplitude of the nth azimuthal pressure mode owing to different physical effects. The first term represents axial tension–curvature effects, the second is wall inertia, and the third term arises due to azimuthal bending. The sum of these three terms matches the overall amplitude of the nth mode pressure forcing Q_n.

This model represents a substantial improvement of previous studies. In the solution method of Whittaker *et al.* (**10**) and Walters *et al.* (**12**), there are two significant limitations that we draw attention to. Firstly, the ad-hoc truncation results in the corrections to the fundamental mode being difficult to calculate, which means that an understanding of the relative error induced by truncating the expansion cannot easily be obtained. Secondly, the pressure is assumed to be azimuthally uniform, which places limitations on future investigation. In the current work, we overcome both of these limitations. The eigenfunction expansion method used here allows the azimuthal modes to completely decouple, meaning that a formal series solution can be obtained, and that an analysis of the error induced after *any* truncation can be constructed trivially. This significant result has allowed us to justify that the leading azimuthal mode provides a dominant contribution to the change in cross-sectional area of the tube. This observation was first made by Whittaker *et al.* (**10**), however they were unable to comprehensively justify such an argument quantitatively due their invoked ad-hoc assumption.

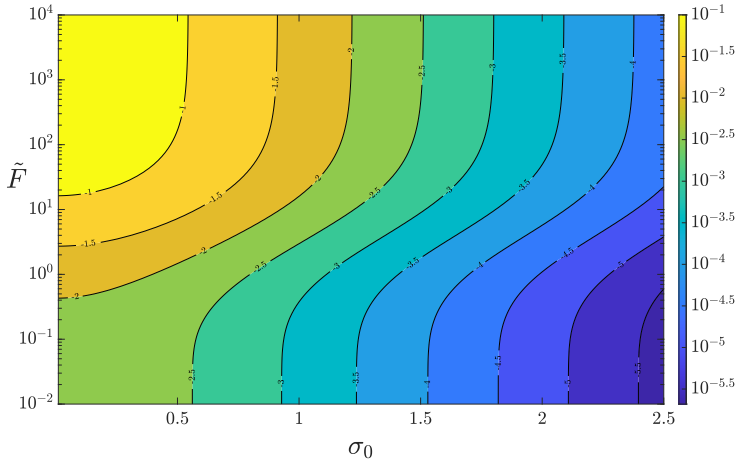

Figure 14: Contour plots of the ratio $\alpha_2(1/2)/\alpha_1(1/2)$ computed using (5.4) for a uniform transmural pressure. This illustrates how changes in $\tilde{F}$ and σ_0 affect the error when truncating the expansion (4.19) after the first mode.

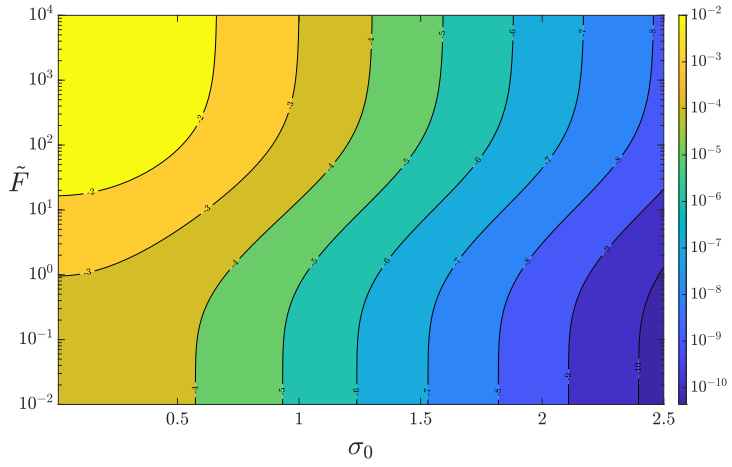

Figure 15: Contour plots of the ratio $\alpha_3(1/2)/(\alpha_1(1/2) + \alpha_2(1/2))$ computed using (5.4) for a uniform transmural pressure. This illustrates how changes in $\tilde{F}$ and σ_0 affect the error when truncating the expansion (4.19) after the second mode.

The 'tube law' like equations (6.1) derived here can be used in a variety of contexts. In this paper we have shown that we can obtain an analytical solution for the case in which the deformations are induced by a steady uniform transmural pressure. We verified that the fundamental azimuthal mode yields the dominant contribution to the change in cross-sectional area, and produced contour plots demonstrating the accuracy of the respective solutions after truncating at the first and second modes throughout different regions of $(\sigma_0, \tilde{F})$ space. For many applications, it is convenient to write (6.1) in terms of the tube's cross-sectional area. For the specific case of coupling the results here to the leading–order fluid mechanics (in which the hydrodynamic pressure is azimuthally uniform) presented in Whittaker *et al.* (**21**), we can write (6.1) in dimensional variables as follows

$$ma\frac{\partial^2}{\partial t^{*2}}\left(\frac{A_n^*}{A_0^*}\right) - \frac{F}{2\pi}\frac{\partial^2}{\partial z^{*2}}\left(\frac{A_n^*}{A_0^*}\right) + \frac{\lambda_n K}{a^3}\left(\frac{A_n^*}{A_0^*}\right) = Q_n^*(z,t)t_n, \tag{6.3}$$

where starred variables represent dimensional quantities. Here F is the dimensional axial tension, K is the bending stiffness, Q_n^* is the forcing from the transmural pressure which can be calculated via (6.2) with $\tilde{P} = p_{tm}^*$, and we have defined A_n^* as the dimensional perturbation to the cross-sectional area associated with the nth azimuthal eigenmode. The total area change is then given by

$$A^*(z,t) - A_0^* = \sum_{n=1}^{\infty} A_n^*(z,t). \tag{6.4}$$

Equation (6.3) can be used to couple the fluid and solid mechanics via the transmural pressure p_{tm}^*. However, at least for the oscillatory problem, the azimuthal modes no longer decouple. Area displacements that are associated with the first azimuthal eigenmode create a pressure distribution in the fluid that forces all of the azimuthal eigenmodes. We can address this limitation by calling on the analysis in the present work that justified a dominant fundamental azimuthal mode. This result means that the dominant contribution to the pressure in the fluid is forced by the $n = 1$ azimuthal mode, and that the response from this pressure is to excite predominantly the first azimuthal mode. Consequently, the coupling with higher order azimuthal modes is weak. The result of this simplification is the ability to compute a series solution.

The ability to permit azimuthal variation into the transmural pressure is significant for future study. Whittaker *et al.* (**21**) derived a model (applicable for the parameter regimes considered here) that couples the wall motion to an internally conveyed viscous fluid. For a regime in which oscillations in the tube wall are of high-frequency and long-wavelength, the tube-law derived by Whittaker *et al.* (**10**) was adequate, since the hydrodynamic pressure was azimuthally uniform at leading-order. To incorporate higher-order effects from the fluid mechanics, we would need to allow azimuthal variation in the transmural pressure, which our results permit.

Whilst the results presented in this paper are developments on previous theoretical and rational descriptions of the Starling resistor, the model is not without its limitations. The action of retaining only leading-order contributions in (2.21) linearises the problem, and therefore non-linear affects (such as instability saturation) are not captured. There are two main draw backs when considering the initial geometry of the tube. In various biomedical

contexts we might expect to find axially non-uniform tubes, whose initial cross-sectional shapes are not necessarily elliptical.

The limitations discussed here provide the foundations for future study. When considering different initial geometries of the tube, it should be relatively straight forward to derive the governing equation (2.21) in terms of an arc-length parameter with an arbitrary curvature $\bar{B}$. Provided that appropriate constraints were placed on the curvature profile of the initial cross-section, one should therefore be able to adapt the solution method discussed here and present solutions for a variety of different cross-sectional shapes. When trying to introduce initially axially non-uniform features (which applies to blood vessels that are partially collapsed) in the tube, more work is required in deriving new governing equations that measure the deformations. One potential avenue might be to capture all of the axial dependence within the ellipticity parameter σ_0.

Acknowledgements

DN would like to acknowledge the financial support of the University of East Anglia to undertake the PhD project of which this work is a part.

References

1. J. B. Grotberg and O. E. Jensen, Biofluid mechanics in flexible tubes. *Annu. Rev. Fluid Mech.* **36** (2004) 121–147.

2. M. Heil and A. L. Hazel, Fluid–structure interaction in internal physiological flows. *Annu. Rev. Fluid Mech.* **43** (2011) 141–162.

3. M. Heil and O. E. Jensen, Flows in deformable tubes and channels. In *Flow Past Highly Compliant Boundaries and in Collapsible Tubes*, pages 15–49, Springer (2003).

4. F. Knowlton and E. Starling, The influence of variations in temperature and blood-pressure on the performance of the isolated mammalian heart. *J. Physiol* **44** (1912) 206–219.

5. A. H. Shapiro, Steady Flow in Collapsible Tubes. *J. Biomech. Engr* **99** (1977) 126–147.

6. J. E. Flaherty, J. B. Keller and S. Rubinow, Post buckling behavior of elastic tubes and rings with opposite sides in contact. *Soc. Ind. Appl. Math.* **23** (1972) 446–455.

7. M. Heil and T. J. Pedley, Large post-buckling deformations of cylindrical shells conveying viscous flow. *J. Fluids Struct.* **10** (1996) 565–599.

8. M. E. Mcclurken, I. Kececioglu, R. D. Kamm and A. H. Shapiro, Steady, supercritical flow in collapsible tubes. Part 2. Theoretical studies. *J. Fluid Mech.* **109** (1981) 391–415.

9. J. Reyn, Multiple solutions and flow limitation for steady flow through a collapsible tube held open at the ends. *J. Fluid Mech.* **174** (1987) 467–493.

10. R. J. Whittaker, M. Heil, O. E. Jensen and S. L. Waters, A rational derivation of a tube law from Shell theory. *Q. J. Mech. Appl. Math.* **63** (2010) 465–496.

11. O. Jensen and T. Pedley, The existence of steady flow in a collapsed tube. *J. Fluid Mech.* **206** (1989) 339–374.

12. M. C. Walters, M. Heil and R. J. Whittaker, The effect of wall inertia on high-frequency instabilities of flow through an elastic-walled tube. *Q. J. Mech. Appl. Math.* **71** (2018) 47–77.

13. R. J. Whittaker, A shear-relaxation boundary layer near the pinned ends of a buckled elastic-walled tube. *IMA Journal of Applied Mathematics* **80** (2015) 1932–1967.

14. M. Walters, *The effects of wall inertia and axial bending on instabilities in flow through an elastic-walled tube*. Ph.D. thesis, The University of East Anglia (2016).

15. W. Flügge, *Tensor Analysis and Continuum Mechanics*. Springer (1972).

16. A. E. H. Love, XVI. The Small Free Vibrations and Deformation of a Thin Elastic Shell. *Phil. Trans. Roy. Soc. London* pages 491–546.

17. P. Blanchard and E. Brüning, *Variational methods in mathematical physics: a unified approach*. Springer Science & Business Media (2012).

18. D. J. Netherwood, *The deformations of elastic walled tubes*. Ph.D. thesis, School of Mathematics, The University of East Anglia. (2022).

19. R. J. Whittaker, S. L. Waters, O. E. Jensen, J. Boyle and M. Heil, The energetics of flow through a rapidly oscillating tube. Part 1. General theory. *J. Fluid Mech.* **648** (2010) 83–121.

20. R. J. Whittaker, M. Heil, J. Boyle, O. E. Jensen and S. L. Waters, The energetics of flow through a rapidly oscillating tube. Part 2. Application to an elliptical tube. *J. Fluid Mech.* **648** (2010) 123–153.

21. R. J. Whittaker, M. Heil, O. E. Jensen and S. L. Waters, Predicting the onset of high-frequency self-excited oscillations in elastic-walled tubes. *Proc. R. Soc. A* **466** (2010) 3635–3657.